

Article

Asymmetric Behavior of Vegetation Seasonal Growth and the Climatic Cause: Evidence from Long-Term NDVI Dataset in Northeast China

Yuke Zhou 

Key Laboratory of Ecosystem Network Observation and Modeling, Institute of Geographic Sciences and Natural Resources Research, Chinese Academy of Sciences, Beijing 100101, China; zhouyk@igsnr.ac.cn

Received: 11 July 2019; Accepted: 6 September 2019; Published: 10 September 2019



Abstract: Land surface phenology is a response of vegetation to local climate and to climate change, leading to crucial impacts on plant growth rhythm and productivity. Differences in vegetation growth activities in earlier and latter parts of the growing season are tightly correlated to phenological changes and the temporal distribution of plant productivity. However, its spatiotemporal pattern and climatic constraints are poorly understood. For Northeast China (NEC), long-term remotely-sensed vegetation greenness records (NDVI) were employed to quantify seasonally asymmetrical characteristics of vegetation growth in detail, which consists of asymmetry in growing rate (AsyR), mean vegetation greenness (AsyV), and growing period length (AsyL) during vegetation green up and senescence stages (simply termed as spring and autumn). Furthermore, the impact of temperature and precipitation on these indices were examined using relative importance analysis. The results indicate these asymmetric metrics present a pronounced interannual variability profile with a potential cycle of ten years (significant in AsyV and AsyR) for the entire NEC. AsyV is changing synchronously with AsyL but asynchronously with AsyR. The geographical distribution of asymmetric indices shows a similar pattern to identified vegetation cover types, especially in distinguishing crops from natural vegetation. Spatial-averaged asymmetric indices indicate spring production is greater than autumn production (reflected by negative AsyV) across most vegetation types in NEC, yet autumn is longer than spring in all vegetation types, which is identified by positive AsyL. Negative AsyR is mainly found in forests implying there is rapid green up and slow senescence in trees. From a temporal perspective, AsyV decreases with time in forested regions but increases in cropland and grassland, which is similar to the pattern for AsyL. AsyR primarily exhibits a positive trend in forest and a negative trend in cropland and grassland. A relative importance analysis indicates that asymmetries of temperature (AsyTemp) and precipitation (AsyPrpc) play an equal role in significantly affecting vegetation asymmetries in greenness and growth rate but are insignificant to growing season length. AsyTemp mainly presents an obvious contribution to changes in AsyR and AsyV over cropland and grassland. AsyPrpc shows a more widespread controlling effect on AsyR and AsyV over the NEC, except in eastern broad-leaved forest. For the entire NEC, asymmetries of temperature and precipitation are negatively correlated with AsyR but are positively correlated with AsyV and AsyL. This finding may imply that a warmer (positive AsyTemp) autumn tends to improve the length and intensity of vegetation activity. Thus, the long-term change in vegetation growth asymmetries may provide insights for the altering functions of ecosystems and provide information to more accurately build plant growth models in the context of global climate change. Additionally, when combined with other information, asymmetric indices can serve as a supporting tool in classification of vegetation types.

Keywords: vegetation growth curve; vegetation phenology; asymmetric indices; remote sensing; GIMMS NDVI3g

1. Introduction

In the northern mid-high latitudes, warming-related shifts in vegetation phenology, particularly to an earlier spring and delayed autumn, and their influence on ecosystem productivity have been extensively reported [1–5]. Currently, remote sensing-based phenological studies focus primarily on changes in key endpoints of phenological events (e.g., dates for spring onset and autumn senescence), through fitting growth curves and extracting phenological parameters [6–10]. Seasonal growth curves will correspondingly change according to phenological shifts. However, our understanding of the detailed variation between vegetation growth activities during green up spring (increasing productivity) and senescence in autumn (decreasing productivity) remains limited over time and space. During this study, we developed a suite of simple asymmetrical indices capable of representing growth distinction between vegetation green onset and offset, as well as estimate their response to climatic change at regional scale in a temperate zone.

Vegetation phenology, one of the most important land surface properties, is used as an essential indicator for depicting global changes [11,12]. It is a key parameter that describe vegetation's growth patterns and is required for modeling land surface processes (e.g., carbon and energy cycles) [11,13]. Currently, remote sensing techniques, from satellites to webcams, provide a continuous way to monitor vegetation phenological cycles at a large spatial scale [6,14]. A considerable number of studies using long-term vegetation greenness indices have found that the earth is becoming more green, especially in the Northern Hemisphere [15]. It is well documented that shifts in vegetation phenological metrics play a key role in regulating greening trends through prolonging the growing season. This extended growing season is directly attributed to both advanced spring onset and postponed autumn ending, further compounding impacts resulting from warming air temperature [16]. Consequentially, these trends affect carbon, water, and energy fluxes between the terrestrial biosphere and the atmosphere [11]. Correlations between phenological metrics and vegetation indices (e.g., greenness, productivity) may overlook impacts from the pattern in the seasonal growth of vegetation, because vegetation greenness phenology metrics are taken at specific points in time and are zero-dimensional data. Furthermore, plant growth processes are affected by a variety of environmental factors that usually lead to changes in these patterns [17]. Thus, distinctive growth patterns for vegetation may result in different allocations of greenness or carbon across the growing season. Green up and senescence rates, peak growth value, and accumulated production are useful information to characterize the seasonal cycle of vegetation. Leonardo Calle et al. proposed a segmentation algorithm for characterizing asymmetries during green up and senescence, investigating its applicability in seasonal XCO₂ data [18]. Long-term trends of global temperature also show a pronounced pattern of seasonal asymmetry [19]. The timing and length of vegetation growth events can influence ecosystem productivity and result in further effects on land surface processes. For instance, seasonal distributions of vegetation productivity can affect food availability for animals, thereby, altering animal migration and breeding patterns. As a result, it is crucial to examine asymmetrical features of vegetation phenology to comprehensively depict vegetation changes and their feedbacks to climate changes.

With the development of methods for extracting phenological metrics based on remote sensing time series data, information can be obtained to characterize plant growth patterns in detail. There are a variety of methods to extract phenology dates from vegetation index time series data. Generally, these methods can be divided into two catalogs: the threshold method and the derivative method [1]. The threshold method simply determines the SOS and EOS (start and end of growing season) using a fixed value (e.g., NDVI) or a fixed percentage of the annual maximum value. The second method captures not only the SOS and EOS when the derivative of the smoothed growth curve is at the local maxima or minima, but also retrieves the time when rates are increasing (decreasing) rate (tangent slope) during green up (senescence) stages [10,20,21]. Thus, the skewness of plant growth patterns can be depicted using the asymmetric features of growing rates. Differences in growing season length and cumulative greenness (or production) during vegetation green up and senescence phases may supply more information to portray phenological asymmetry. These variables can be seen as comprehensive

phenological parameters, and their changes can differentially alter plant functions, affecting carbon, water, and energy fluxes between the terrestrial biosphere and the atmosphere.

With extensive studies based on field data, satellite images, and ecosystem process models, it has become evident that the response of plant phenology to climate variability and change is both location- and species-specific [22–25]. Thus, it would be more meaningful to focus the investigation on vegetation growth changes at the regional scale than at the global scale. Northeast China (hereafter NEC), a typical temperate zone in the mid-latitudes, has a variety of vegetation types, including forests (evergreen needleleaf forest, deciduous needleleaf forest, deciduous broadleaf forest, and mixed forests), croplands, and grasslands [26]. It has proven to be a suitable area for studying shifts in vegetation phenology and concomitant climatic feedbacks [26–28]. Furthermore, the availability of numerous satellite datasets, such as GIMMS NDVI3g, Modis NDVI and Spot VGT, enable us to explore vegetation phenology changes and climatic impacts across a long time period for Northeast China [29–31].

In this study, long-term vegetation greenness data from GIMMS NDVI3g was adopted to derive key vegetation phenological metrics (start, end, peak, growth rate, and duration of the growing season), to generate asymmetrical growth indices across the NEC. Next, the strength and spatial pattern of asymmetries in regional location, plant type and temporal were investigated. Thereafter, detailed patterns of vegetation asymmetry responses to changes in climatic forces (temperature and precipitation) were examined using correlation analysis. Finally, the utility of these detailed asymmetrical indices depicting vegetation growth cycles and their climatic implications were discussed.

2. Study Area, Data and Methods

2.1. Study Area

This study was carried out in Northeast China (NEC), comprised of Heilongjiang, Jilin, Liaoning and parts of Inner Mongolia provinces (Figure 1). This region is 115×10^4 km² in area, accounting for 15% of the national territorial area of China. Latitude and longitude for the NEC range from 115°E~135°E and 38°~56°N, respectively. Its terrain is primarily composed of three parts: mountainous areas, hills, and plains (Figure 1a). The mountainous areas are mainly distributed across the northern and eastern parts. The central and northeast sections are dominated by the Songnen Plain and the Sanjiang Plain, respectively. The elevation of the NEC ranges from 0 to 2667 m, with lower elevations found in the northeast, south, and west, and higher elevations in the north, east, and southeast (Figure 1a). Much of the region belongs to a temperate zone characterized by a continental monsoon with four distinct seasons (cold in the winter and warm in the summer). Annual precipitation decreases from east to west, varying from 400 to 800 mm; a similar trend exists for relative humidity. NEC has a high proportion of vegetation cover, including temperate forests, grasslands and agriculture (Figure 1b). The coniferous forest is distributed in the northern mountain area (Daxing'anling), while broad-leaved forests are located in the eastern and southern parts. The central and eastern plains are covered by croplands.

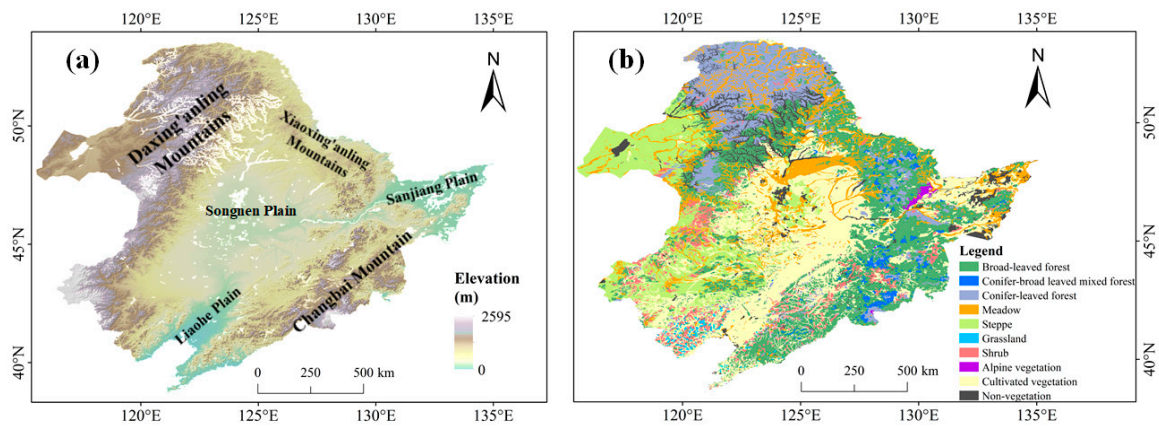


Figure 1. Topographic map (a) and vegetation types (b) in Northeast China.

2.2. NDVI and Meteorological Dataset

Long-term satellite data of vegetation greenness using NDVI, a proxy for potential photosynthesis closely related to plant productivity, were used to estimate the sign and magnitude of asymmetric patterns of growth during the growing season. The NDVI dataset used in this study (NDVI3g V1) was produced by the GIMMS group using a series of NOAA-AVHRR satellite imagery (<https://ecocast.arc.nasa.gov/data/pub/gimms/>) [29,30]. It covers the period 1982–2015 with a temporal resolution of 15 days at 8 km spatial resolution. This NDVI3g product has been used extensively since being published and is the most consistent long-term satellite vegetation dataset currently available [30]. In this version of NDVI, effects of orbital drifts, inter-sensor calibration and aerosol impacts from volcanic eruption have been corrected. The region of Northeastern China was extracted from each image in the raster data stack. Grid cells with NDVI values less than 0.1 were masked out as bare land, water, or urban areas.

It has been well documented that climate change plays a key role in affecting long-term changes and variability in vegetation [20,32]. In this study, to quantify climatic effects on the asymmetries in vegetation seasonal cycle, a suite of spatially gridded temperature and precipitation data were employed. These datasets were obtained from Wang, et al. [33] (<http://www.csdata.org/en/p/80/>) and cover the study area spanning the time period of 1982 to 2015. Temperature and precipitation datasets with a grid resolution of 1 km were produced from observed surface data obtained from the National Meteorological Information Center (NMIC) of China Meteorological Administration. Wang, et al. then calculated eight-day average and total values for temperature and precipitation, respectively, to match the temporal frequency of MODIS data. The ANUSPLIN software was used to interpolate observed meteorological data to a grid with high resolution (1-km), and the results were validated with temperature and precipitation records from AsiaFlux stations (<http://asiaflux.net>). In this study, the spatial resolution of temperature and precipitation data was resampled into an 8 km grid using the nearest neighbor method in ArcGIS 10.3. Using this data, temperature and precipitation asymmetry were calculated in the same manner as the vegetation asymmetric indices.

2.3. Extracting Phenological Metrics

The Double Logistic Function (D-L) curve method was used to reconstruct the NDVI time series data in Northeast China (NEC) from 1982 to 2015, and the vegetation phenological parameters were extracted using the curvature method [20]. These parameters included the start of growing season (SOS), the end of growing season (EOS), maximum growth activity date (PEAK position), length of growing season (LOS), green up rate (RSP) and senescence rate (RAU) (Figure 2). RSP and RAU are crucial phenological metrics for depicting growth rate, which have not received adequate attention in previous studies of plant phenology. Spatiotemporal patterns of RSP and RAU, as well as their

implications for vegetation activity during growth transition periods remain poorly understood. The growth curve fitting and phenological parameter extraction formulas are as follows:

$$\text{NDVI}(t) = (\text{mNDVI} - \text{wNDVI}) \left(\frac{1}{1 + e^{-mS(t-S)}} + \frac{1}{1 + e^{-mA(t-A)}} - 1 \right) + \text{wNDVI} \quad (1)$$

where $\text{NDVI}(t)$ represents the NDVI value at the t th day of year (DOY), wNDVI and mNDVI are the NDVI in winter and the maximum NDVI in peak position during plant growth process, respectively. S and A stand for the inflection points on the curve rising and falling process, and mS and mA are the rate of curve increasing or decreasing at the inflection point (RSP and RAU). The NDVI value in winter, termed as wNDVI , was determined using the following equation:

$$\text{wNDVI} = \sqrt{\max(\text{NDVI}_{10}) \times \max(\text{NDVI}_{11})} \quad (2)$$

where NDVI_{10} and NDVI_{11} represent the NDVI values in October and November, respectively. Except for wNDVI , parameters were calculated using the iterative nonlinear least squares method. The curvature was obtained using the NDVI fitting curve, and the curvature formula was derived from this. When the derivative is zero, the curve is the greatest. This point was defined as a phenological transition period (SOS and EOS) during vegetation growth [20]. The R package 'greenbrown' was used to obtain these phenological metrics [34].

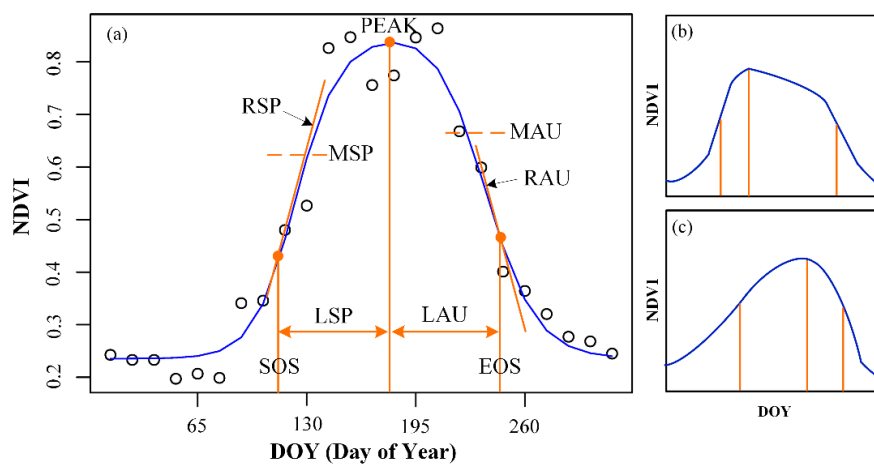


Figure 2. Conceptual illustration of vegetation growth asymmetries (a) symmetrical type; (b) rapid in and slow out; (c) slow in and rapid out.

2.4. Definition of Phenological Asymmetry Indices

In the context of global warming, the seasonal cycle of vegetation growth has shown a pronounced shift in both spatial and temporal patterns in northern terrestrial ecosystems. Here, given vegetation growth for a single growing season in the NEC, three growth asymmetry indices were defined based on the difference between key phenological characteristics for the green up and senescence phases. The green up phase corresponds to the first half of the growing season spanning spring to early summer, followed by the second phase, senescence, spanning early summer to late autumn. The two phases were separated by the position of peak growth (Figure 2). Indices consisted of asymmetries for growing season length (AsyL), green up rate and senescence rate (AsyR) and average NDVI (AsyV) for the two stages of growth. Owing to the distinct sign of these parameters (positive RSP and negative RAU), each asymmetry index was calculated as the difference of absolute values for growth parameters in spring and autumn (Equation (3)). LSP and LAU represent growing season length in spring and autumn, respectively. Similarly, MSP and MAU correspond to the mean value of vegetation greenness index (NDVI) during green up (predominantly spring) and senescence (predominantly autumn). RSP

and RAU indicate the maximum growth rates during green up and maximum declining rate during senescence, respectively. As a result, the sign of the asymmetry index, either positive or negative, can be an indicator of skewness in vegetation growth morphology during spring and autumn. Meanwhile, the magnitude of the asymmetry index represents different levels of vegetation activity during the two stages.

$$\begin{aligned} \text{AsyL} &= |\text{LAU}| - |\text{LSP}| \\ \text{AsyR} &= |\text{RAU}| - |\text{RSP}| \\ \text{AsyV} &= |\text{MAU}| - |\text{MSP}| \end{aligned} \quad (3)$$

Based on the skewness of plant growth asymmetry indices and the condition of vegetation for a single growing season across NEC, plant growth asymmetric features in one year are classified into three common forms: (1) symmetrical pattern for green up and senescence phases (weak asymmetry, Figure 2a); (2) ‘rapid growing and slow declining’ pattern (Figure 2b), reflecting the rapid growth in spring and slow senescence in autumn; (3) ‘slow growing and rapid declining’ pattern (Figure 2c), indicating slowly gradual green up and rapid senescence. The symmetrical growth pattern is reflected in small values of asymmetric indices. In other words, a smaller value of an asymmetric index represents a more pronounced symmetrical pattern in vegetation growth. Given a relatively fixed growing season controlled by internal plant mechanisms for the type 2 growth cycle, the AsyL index will show a positive value due to the earlier arrival of peak growth. In contrast, the AsyL index has a negative value. The signs of AsyV and AsyR cannot be easily determined without additional information. Their long-term trends and variability were investigated at pixel and vegetation cover regional levels as described in the following section.

These growth types may not only be attributed to the genotype of plants but may also be influenced by environmental factors such as temperature, precipitation, and soil water stress. On one hand, using these asymmetric indices, the inherent property of vegetation growth rhythm could help to identify different vegetation cover types. On the other hand, the variability of changing climate can alter the distinct growth status in spring and autumn. Optimal combinations of natural factors will enhance vegetation activity; alternately, less desirable environmental conditions disturb the regular pace of vegetation growth. Changes in natural factors, such as extreme events in rainfall or temperature, may occur at different times during the growing season. Vegetation growth processes adapt to environmental changes, resulting in diversity in growth curves across years. Detailed impacts of climatic factors on the long-term changes of asymmetric indices, and the corresponding spatiotemporal pattern are explored and discussed in subsequent sections.

2.5. A Trend and Correlation Analysis

The Mann-Kendall (MK) trend test, as a non-parametric test, is suitable for handling non-normally distributed data and has been extensively used to examine long-term trends for meteorological, hydrological, and land surface vegetation parameters [35–37]. The MK test does not require normality when processing time series data and is insensitive to outliers. With the MK trend test and a time series with n observed data ordered by time sequence (x_1, \dots, x_n) , the null hypothesis H_0 states that the series does not show a monotonic trend, and the alternative hypothesis H_1 indicates there is an obvious monotonic trend. For all $k, j \leq n$ ($k \neq j$), the key statistical variable S (Equation (4)) is tested.

$$S = \sum_{k=1}^{n-1} \sum_{j=k+1}^n \text{sgn}(x_j - x_k) \quad (4)$$

$S > 0$ indicates that the latter observation tends to be greater than the former one, and $S < 0$ denotes the opposite. The variance $\text{VAR}(S)$ is calculated (Equation (5)), where g is the number of groups, and tp is the number of observed values in the p -th group.

$$\text{VAR}(S) = \frac{1}{18} [n(n-1)(2n+5) - \sum_{p=1}^g t_p(t_p-1)(2t_p+5)] \quad (5)$$

Finally, the Mann-Kendall statistical value ($_{mk}$ tau) is obtained, which is represented by Z_{mk} (Equation (5)). The Mann-Kendall tau coefficient ranges between -1 and $+1$. A positive value implies an upward temporal trend, whereas a negative value implies a decreasing trend.

$$\begin{aligned} Z_{mk} &= \left| \frac{S-1}{\sqrt{\text{Var}(s)}} \right|, S > 0 \\ Z_{mk} &= 0, S = 0 \\ Z_{mk} &= \left| \frac{S+1}{\sqrt{\text{Var}(s)}} \right|, S < 0 \end{aligned} \quad (6)$$

Correlations between the time series of plant asymmetric indices and climatic data are assessed using Spearman rank-order correlation coefficients, a nonparametric method used to evaluate the monotonic relationship between two continuous or ordinal variables. The concrete process for calculating Spearman correlation coefficients is further described elsewhere [38,39].

2.6. Relative Importance Analysis

In this study, temperature and precipitation were used to explore environmental impacts on vegetation growth asymmetries. Like the definition of vegetation asymmetry, the term *AsyTemp* (*AsyPrcp*) is defined to depict the difference in average temperature (summed precipitation) between the first and second half of the growing season (same period as for vegetation asymmetry), which is determined using the SOS, POP and EOS identified for phenological parameters. In Equation (7), τ_{Pau} and τ_{Psp} represent temperature (precipitation) in green up (spring) and senescence (autumn) seasons, respectively.

$$\begin{aligned} \text{AsyTemp} &= \tau_{\text{Pau}} - \tau_{\text{Psp}} \\ \text{AsyPrcp} &= \text{Pau} - \text{Psp} \end{aligned} \quad (7)$$

A relative importance (RI) approach is utilized to quantify their respective contribution to long-term changes of plant growth asymmetries in each grid cell. This method is expressed as a multiple linear regression (Equation (8)). There, *AsyVeg*, representing *AsyV*, *AsyL* and *AsyR* (dependent variable), is regressed against *AsyTemp* and *AsyPrcp* (independent variable). ϵ indicates drivers that are not mentioned but might contribute to variations in plant growth asymmetry. Relative importance was implemented using the 'relaimpo' package in R [40], which is based on variance decomposition in multiple linear regression models.

$$\text{AsyVeg} = \beta_0 + \beta_1 \times \text{AsyTemp} + \beta_2 \times \text{AsyPrcp} + \epsilon \quad (8)$$

when the coefficient of determination (R^2) for the above multiple regression was obtained, it is decomposed into non-negative contributions shared by each variable in the following formula (lmg method in 'relaimpo' R package [41]). The RIs of multiple variables sum to the total R^2 where x_k represents *AsyTemp* or *AsyPrcp* ($k = 1, 2$), and p equals 2. The $\text{seq}R^2$ denotes the additional R^2 when adding the regressor x_k to a model with the regressors in set S . Thus, $\text{LMG}(x_k)$ is the RI for *AsyTemp* or *AsyPrcp*.

$$\text{LMG}(x_k) = \frac{1}{p} \sum_{j=0}^{p-1} \left(\sum_{\substack{S \subseteq \{x_1, \dots, x_p\} \setminus \{x_k\} \\ n(S) = j}} \frac{\text{seq}R^2(\{x_k\}|S)}{\binom{p-1}{j}} \right) \quad (9)$$

3. Results

3.1. Spatiotemporal Pattern of Growth Asymmetric Indices

3.1.1. Interannual Variability of Vegetation Asymmetries for NEC

To ascertain the overall status of vegetation asymmetries for NEC, regional average annual asymmetric indices are calculated. Then the corresponding interannual variation was obtained from the time series (Figure 3). The three indices have an evident cycle in their time series, but the periodic phases are variable. To accurately quantify the cycle period, the dominant frequency of vegetation asymmetries is determined from a spectral analysis of the time series (using R package ‘forecast’) [42]. This procedure revealed that the dominant frequency of AsyV, AsyR is 11 and 10 years, respectively. The periodicity of AsyV and AsyR is statistically significant and is also reflected by obvious periods in the time series plot, such as 1982–1992 and 2003–2013. AsyL has a relatively large interannual fluctuation and does not exhibit a remarkable period, but visually there is a shorter period that is around eight years (not to be identified by spectral analysis). The directions of amplitude in AsyV and AsyR show an opposite pattern, in other words, AsyV decreases with the increasing AsyR. Generally, AsyL keeps a consistent phase with changes in AsyV but with remarkable fluctuation. Prior to 2000, trends and periodic characteristics of the three indices are relatively prominent. During the subsequent time interval, their inter-annual variability increases, and the amplitudes tend to decrease, which may be associated with changing climatic factors such as the global warming slowdown after 1998 [43,44].

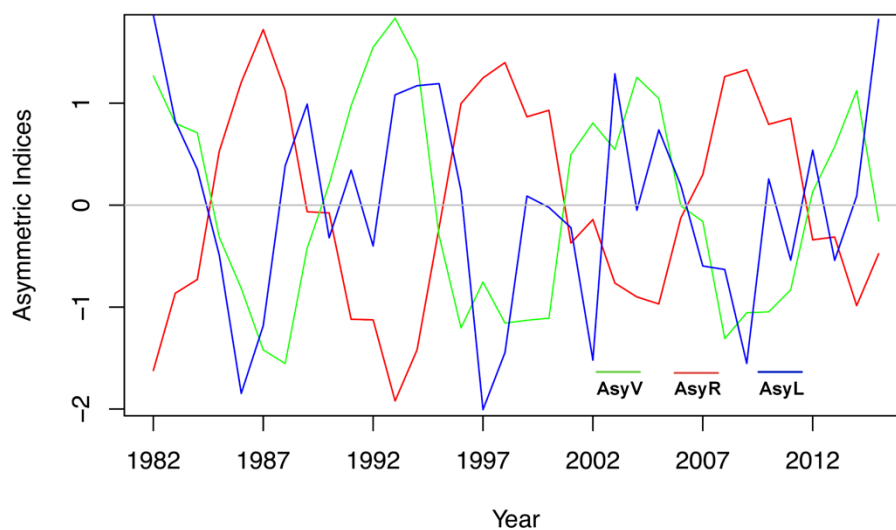


Figure 3. Interannual variations in vegetation growth asymmetries for the entire Northeast China (NEC). For better graphical presentation, raw annual time series were normalized.

Across the entire NEC, correlations between the three asymmetric indices (AsyL, AsyV, AsyR) were assessed using Spearman correlation analysis. The results show that AsyR and AsyV have a negative correlation (Spearman $r = -0.67$), meaning that if in the trend in AsyR continues to increase (vegetation consistently shows a pattern of slow increase during green up and rapid decrease during senescence), the difference in vegetation activity between the two time periods (AsyV) will decrease. In other words, rapid senescence of vegetation in autumn would result in decreased productivity, thus reducing its impacts on annual productivity as compared to spring productivity. Consistency between AsyV and AsyL indicates that an extension of the senescence window when compared to green up contributes to an increase in autumn vegetation productivity. Due to inherent variability, AsyL is weakly correlated with AsyV (Spearman $r = 0.48$). AsyR and AsyL show a strongly negative correlation (Spearman $r = -0.81$), reflecting that a rapid decrease in vegetation greenness will shorten the duration of senescence.

Like the temporal distribution, spatial distributions of average annual AsyV and AsyR demonstrate a regular patch pattern that matches vegetation cover types (Figure 4b,c). The map of average AsyL shows a relatively discrete pattern (a weak cluster status) (Figure 4a). Across the NEC, spatially averaged AsyL and AsyR show positive signs, while AsyV has a small negative value (-0.01). In other words, the late growing period overwhelms the early growing period in controlling total annual growing season length, identified by the positive AsyL occurring in each vegetation type (Figure 4d). Positive AsyL is most statistically significant in grassland and alpine vegetation. At the pixel scale, negative AsyL values can be found in northern and southeastern natural vegetation. AsyV is positive in conifer-leaved forests but is negative in other vegetation types, indicating again that productivity during senescence plays a dominant role in annual productivity for many regions of the NEC (Figure 4e). Grasslands have the most negative values for AsyV, followed by croplands and alpine vegetation.

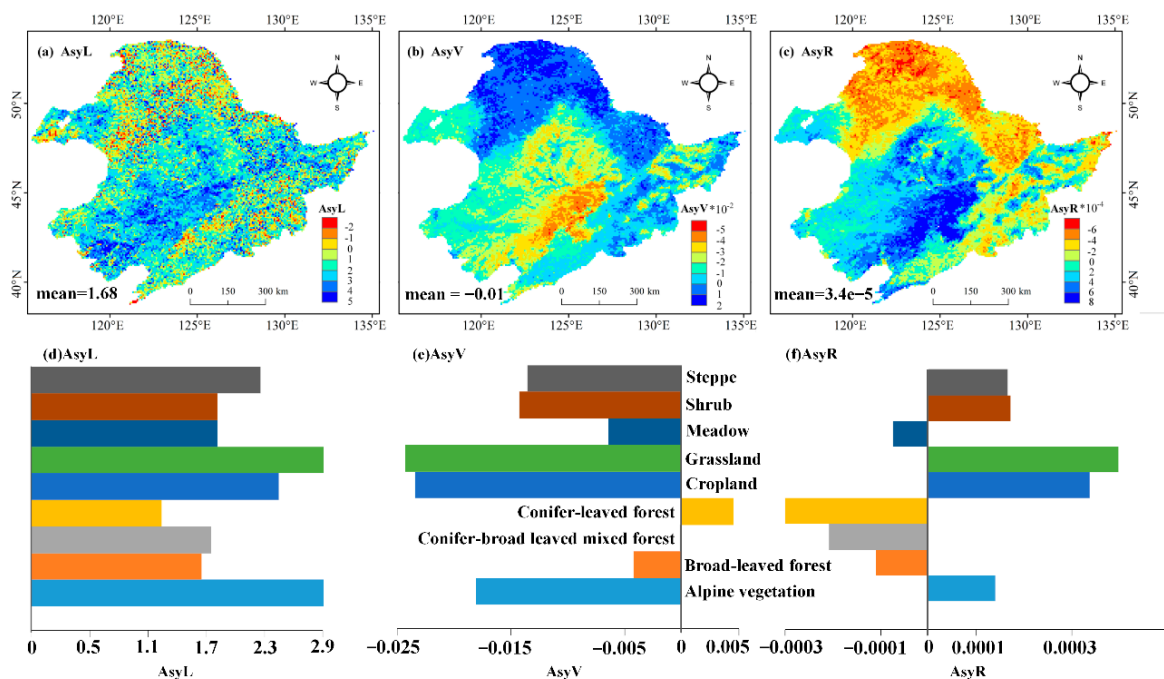


Figure 4. Spatial distribution of multi-year averaged asymmetric metrics (a–c) and statistical distribution (d–f).

3.1.2. Long-Term Trends

Long-term trends in the three asymmetry indices were analyzed using the Mann Kendall trend test (expressed as MK tau values, Figure 5). The spatial heterogeneity of AsyL trends is still pronounced in that most northern coniferous forests show a positive trend, while some broad-leaved forests in the east, grasslands in the west, and croplands in the south display negative trends. Similar to the average annual metrics (Figure 4), spatial patterns of trends in AsyV and AsyR are also significant. A majority of cropland AsyV values have positive trends, indicating that cultivated vegetation activity during green up in the spring tends to have an advantage over senescence in the fall in the long run. Meanwhile the dominant negative trends of AsyV in coniferous forest in northern NEC indicate that vegetation activity during green up would continue to have a greater impact than senescence in autumn. AsyR has a negative trend for most of the cropland, meaning that, in the future, senescence in autumn will become slower than green up in spring. AsyR in natural vegetation has a positive trend, reflecting that the rate during autumn senescence will continue to be stronger than the green up rate in spring.

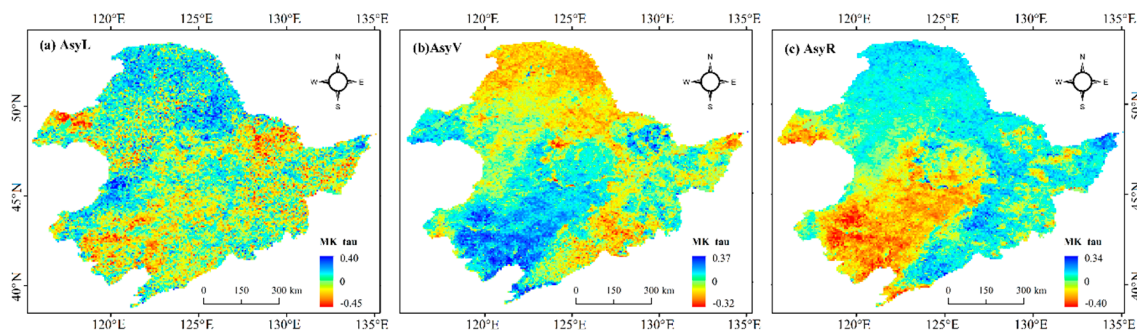


Figure 5. Spatial distribution of long-term trends of vegetation asymmetries (mk tau).

Trends in the asymmetric metrics for each vegetation cover type demonstrate substantial variability (Figure 6). It is noteworthy that there are more vegetation cover types with negative trends than with positive trends (18 vs. 9). Prevailing negative trends in these asymmetric indices may imply that vegetation growth cover types in NEC will be stable into the future, but trends for the three asymmetric indices do not show a consistent pattern for each vegetation cover type. Positive trends are primarily seen with AsyR and AsyV. Only AsyV shows a positive trend in the grassland, steppe and cultivated (cropland) vegetation areas. AsyR shows a positive trend in meadows, alpine vegetation, broad-leaved forests, coniferous-broad leaved mixed forests, and coniferous forests. AsyL only shows a positive trend in coniferous forests. In terms of the magnitude of change, AsyV and AsyR show the largest positive and negative MK trends in the grassland biome. The trend for each index in shrublands is relatively small, probably due to its small, discrete coverage that is insufficiently sensitive to the coarse spatial resolution of satellite data. In addition, AsyL and AysR show negative trends in grassland, steppe and cropland areas, whereas AsyV has a positive trend, indicating that vegetation growth during green up tends to be longer than growth during the senescence period in autumn. Overall vegetation production, however, is still controlled by the senescence period. The multi-year trend of AsyR in meadow, broad-leaved forest and coniferous broad-leaved forest is negative, while AsyL and AsyV in these cover types show an increasing trend.

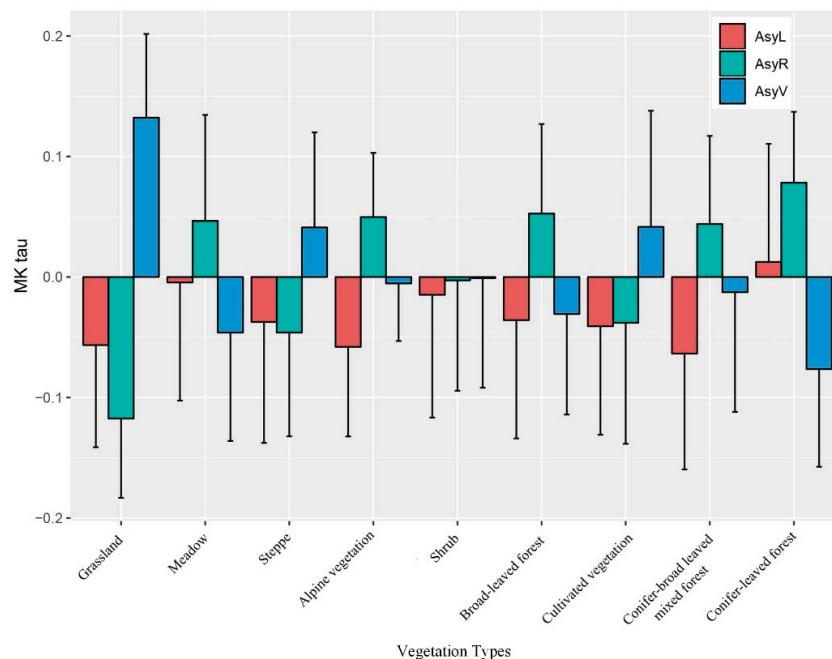


Figure 6. Statistics of asymmetry trends for various vegetation cover areas (averaged value + one standard deviation).

3.2. Correlation between Three Asymmetry Indices

The three asymmetric indices are designed to reveal the detailed diversity of vegetation growth during the increasing and decreasing productivity stages based on phenological signals and direct vegetation greenness status. To examine whether these indices are consistent with each other and can jointly explain the asymmetric features in vegetation growth throughout the growing season, the Spearman correlation analysis is conducted at pixel scale (Figure 7). The spatial pattern of correlation coefficients shows that the three indices are not significantly related to each other in the central portion of NEC that is mainly covered by cropland. This phenomenon may be a consequence of the variable growth process of crops influenced by human management activities. For instance, irrigation offsets water deficits during the arid spring thus enhancing vegetation growth. Additionally, fertilization added to the soil at various times may provide sufficient nutrients to improve growth of cultivated vegetation. Many more pixels show a negative relationship between *AsyL* and *AsyR*, which is particularly pronounced in the southeastern broad-leaved forest (Figure 7a). In other regions with natural vegetation, *AsyL* and *AsyR* have low correlations (around $-0.4\sim 0.2$). *AsyL* is negatively correlated with *AsyV* in most areas of natural vegetation, with the exclusion of the eastern broad-leaved forest. Strong, negative relationships between *AsyL* and *AsyV* were found in the northern coniferous forest and steppe in the western part (Figure 7b). Compared to *AsyL*, *AsyV* has a more evident correlation with *AsyR* reflecting from the spatial distribution. For *AsyR* and *AsyV*, a dominant number of the significant pixels show a strong negative relationship, especially in the northern coniferous forest and western broad-leaved forest (Figure 7c).

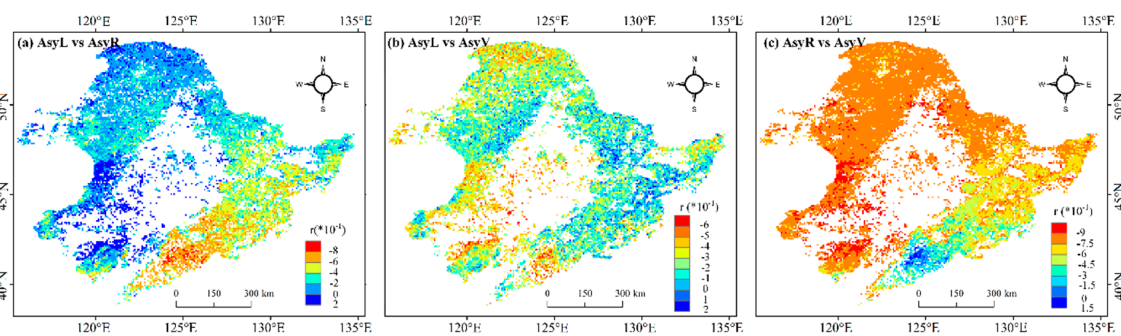


Figure 7. Spatial distribution of correlation coefficient of three asymmetric indices (white cells denote insignificant correlations).

3.3. Climatic Impacts on Vegetation Asymmetry Indices

3.3.1. Interannual Variability of Asymmetries in Temperature and Precipitation

Understanding the climatic constraints that underly seasonal change in plant growth is crucial for explaining climate change effects on global vegetation productivity. Across the entire NEC, results show that *AsyTemp* and *AsyPrcp* exhibit remarkable interannual variability (Figure 8). The temporal dynamics of *AsyTemp* and *AsyPrcp* do not appear to have a significant cyclicality, but fluctuations in these variables are both positive and negative. These changes in *AsyTemp* and *AsyPrcp* imply that seasonal distribution of temperature and precipitation do not consistently play a major role in controlling the interannual variability in vegetation growth. The fluctuating profile of the *AsyTemp* time series is consistent with that of the *AsyPrcp* time series, which is also reflected by their high correlation coefficient of 0.8 (Figure 9). More specifically, the obvious peaks around 1992 and 2003 for the two time series generally match each other. The negative amplitude in *AsyTemp*, on the other hand, is relatively larger than that in *AsyPrcp*.

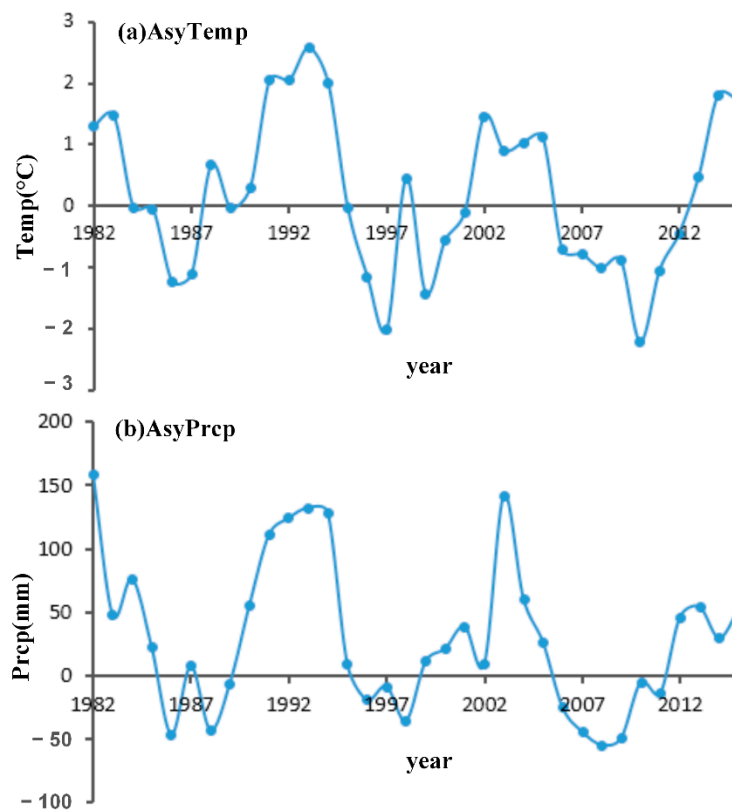


Figure 8. Interannual variability of asymmetries for temperature (a) and precipitation (b).



Figure 9. Correlation matrix among the asymmetry time series for temperature, precipitation and vegetation growth asymmetries over the entire Northeast China (NEC) (blank block denotes insignificant correlation).

To compare asymmetries in temperature and precipitation with those in vegetation growth, their relationships were quantified using Spearman correlation analysis, at the scale of the NEC (Figure 9). The results suggest that AsyTemp does not have a significant relationship with AsyV ($r = 0.42$), but it does have a significant positive correlation with AsyL (-0.81) and a large, significant negative correlation with AsyR (-0.95). AsyPrcp is related to all the vegetation asymmetric indices, with its

most substantial positive relationship being that with AsyL (0.69) and its largest negative relationship (-0.83) being that with AsyR. AsyPrpc exhibits a weaker correlation with NDVI asymmetry (0.59).

At the pixel level, averaged asymmetries for temperature and precipitation across the NEC exhibited a slightly similar spatial pattern, with apparent clusters (Figure 10) where positive AsyTemp and AsyPrpc are distributed widely within natural vegetation in the northern and eastern areas. There is a positive AsyTemp for approximately 55% of the vegetated area. Negative AsyTemp accounts for 45% of the area, which is primarily found in the central agricultural lands. Negative values are shown for 19% of AsyPrpc and are mainly clustered in the southwestern NEC. Using the multi-year mean, precipitation has a greater impact later in the season, after the peak rather than before it.

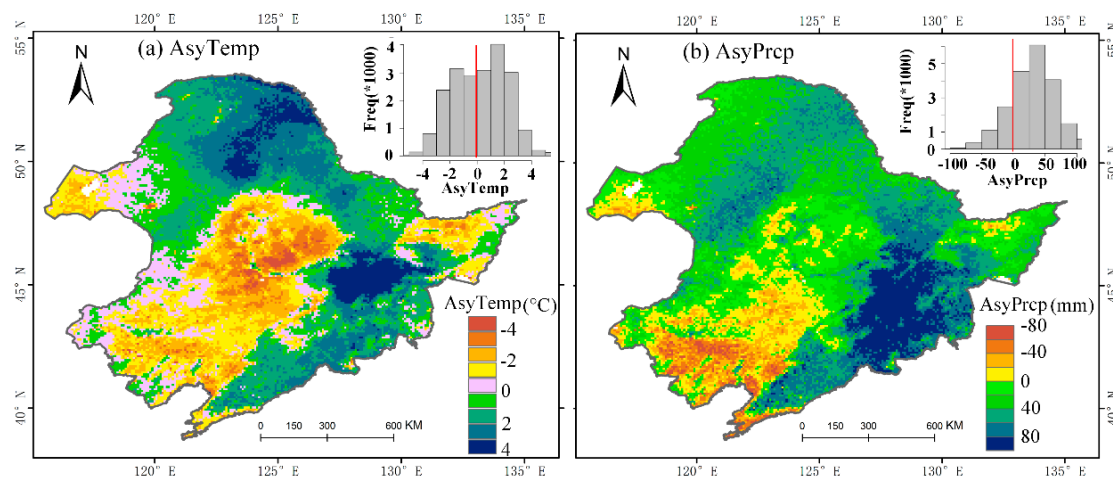


Figure 10. Maps of asymmetry for temperature and precipitation (1982–2015 multi-years average).

3.3.2. Climatic Effects on Vegetation Asymmetries

To estimate climatic controls on seasonal difference in plant growth, the relative importance (RI) of the temperature and precipitation asymmetries on vegetation growth asymmetries was calculated using a linear regression model (Equation (8)). For the entire region, this analysis confirms that AsyTemp and AsyPrpc account for 37.1% and 37.5% of the change in AsyV, respectively. The corresponding proportion of variance explained by the model is 74.6%. The equivalent relative contribution of AsyTemp and AsyPrpc to AsyR (AsyL) are 37.5% (12%) and 41.8% (23%), respectively. These RI results suggest that asymmetry of precipitation provides a slightly larger contribution to the asymmetry of vegetation growth. Conversely, the difference in growing season length between green up and senescence is not strongly influenced by AsyTemp and AsyPrpc, which together only explain 35% of the variations in AsyL.

Similarly, a relative importance (RI) analysis was performed at the pixel level to detect any geographic pattern of climatic impacts on vegetation asymmetries (Figure 11). Geographically, the RI of AsyTemp to AsyR and AsyV tend to show an inverse pattern, as shown by the contrasting yellow and green colors in central and northern NEC. Across the entire area, the magnitude of the RI for AsyTemp on AsyR and AsyV is nearly identical (25% vs. 24%). AsyPrpc has more influence on differences in the growth rate (AsyR) than in greenness (AsyV) during senescence (31% vs. 24%). Spatially, asymmetries in temperature and precipitation do not supply a significant contribution to changes in vegetation asymmetries across the eastern broad-leaved forest. Growing season length (AsyL) is weakly affected by AsyTemp and AsyPrpc, as indicated by the corresponding small RI values widespread across the NEC (total mean value of 3.8% for AsyTemp and 8.7% for AsyPrpc). Their complex spatial heterogeneities (Figure 11e,f) are consistent with the average annual AsyL (Figure 4) and long-term trends in AsyL (Figure 5).

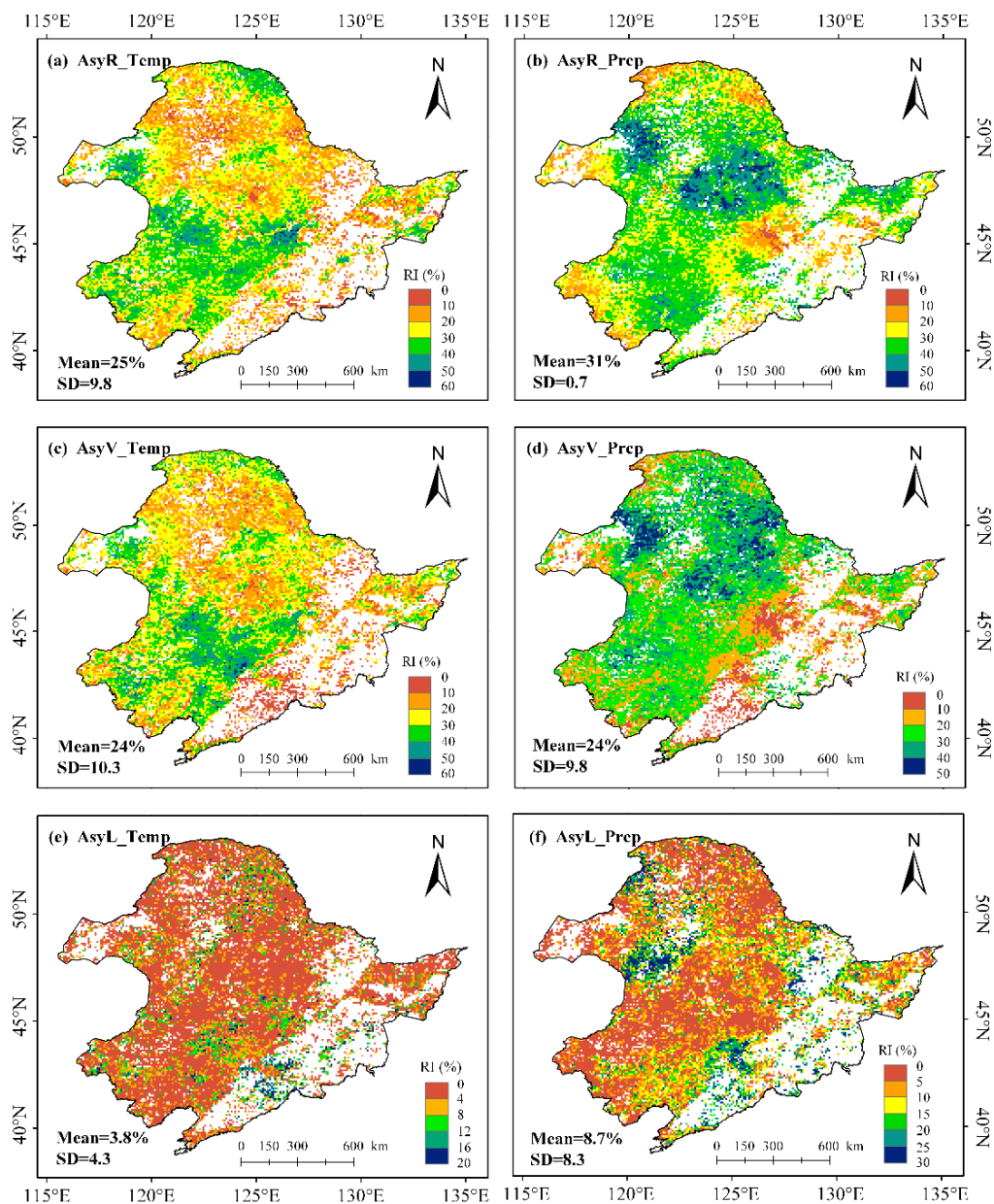


Figure 11. Spatial patterns of relative contribution of asymmetries in temperature (the first column) and precipitation (the second column) to vegetation growth asymmetries (in rows) at pixel scale (white grids are insignificant). RI denotes relative importance.

4. Discussion

4.1. Interpretation of Asymmetries for Depicting Vegetation Cycle

Since vegetation asymmetric indices are not typical variables for characterizing seasonal difference in plant growth, it is necessary to discuss their potential and implications of their use in describing vegetation seasonal cycles. These asymmetric metrics are designed to measure the degree of skewness of the vegetation growth process that typically represents a single growing season. Here, the asymmetry of the vegetation growth curve is expressed by the difference in growth rate (AsyR), growing season length (AsyL), and vegetation activity (i.e., greenness; AsyV) before and after the peak of growing season. The rising segment of the growth curve corresponds to the vegetative green up process. Thus, the green up rate captures information about plant activity, such as leaf development or increasing photosynthesis. In contrast, the declining rate in autumn reflects vegetation browning or senescence.

Differences between the length of active growing season during these two periods are denoted by the asymmetric index *AsyL*, which is tightly correlated to the start of season (SOS), peak of growing season, and end of season (EOS). Thus, *AsyL* reflects the dynamics of phenological events, or differences in timing of carbon uptake [45]. Furthermore, given the relatively fixed lifespans of leaves in northern ecosystems [46], the position of peak vegetation activity plays a key role in controlling the asymmetry of vegetation seasonality, which determines the allocation of plant production to green up period and senescence period. Furthermore, the inherent characteristic (e.g., vegetation gene type) of terrestrial biosphere may be a more dominant driver of growing season asymmetry [18]. For *AsyV*, it is the difference between averaged greenness in the first- and second-half of growing season, so *AsyV* could reflect the capacity of vegetation photosynthesis or production.

By constructing these asymmetric indices, information about annual cycles of vegetation development is retrieved. In general, the indices serve as a set of advanced phenological traits for north ecosystem. Gu et al. suggested that plant photosynthetic seasonal cycles could be seen as an extension of plant phenology. Potential uses of these asymmetric indices include examining regulation of phenophase in land surface productivity models and monitoring vegetation response to interannual climatic variability. In the long run, changes in the seasonal cycle of plants and the asymmetrical characteristics of the growing season have many consequences for ecological processes, agriculture, and forestry. For example, thriving plants in spring are able to provide adequate food for birds and insects thus will enhance ecosystem biodiversity, but sparse plants in spring will affect the livelihood of various animals. Furthermore, vegetation status can affect land surface albedo, thus *AsyV* may influence the temporal distribution of energy between spring and autumn. In this study, long-term *AsyV* and *AsyR* show a pronounced cycle that reflects variability in vegetation photosynthesis, which further reveals that there is not a constant trend in which the green up or senescent phase consistently dominates plant production. The fluctuation of vegetation asymmetries also represents the adaptability of plants to environmental changes.

4.2. Implication for Land Cover Classification

Vegetation phenology also represents a potentially significant source of land cover information [47]. To some degree, asymmetric indices are able to distinguish between natural and cultivated vegetation, especially as shown in the geographic distribution of *AsyR* and *AsyV* (Figure 4b,c and Figure 5b,c). That may be attributed to the inherently phenological features of specific species, as well as human activities (e.g., irrigation, fertilization, harvesting etc.), but it is merely an approximate matching of *AsyR* and *AsyV* to the different vegetation types. Asymmetric indices may be capable of classifying vegetation types through developing more growth curve shape parameters and using datasets with high spatiotemporal resolution (e.g., daily carbon flux, web camera images). Previous studies also confirmed this point using eddy flux records to explore seasonal patterns of net carbon exchange in various forest types [27]. Similarly, other analyses based on multitemporal remote sensing data with high spatial resolution (e.g., Landsat, MODIS) have obtained credible results in vegetation classification that primarily use various plant phenological indicators [48–51]. These studies confirm the potential use of asymmetric indices in land cover classification, but advances are needed, requiring new data sources and more refined methods. Overall, asymmetric indices are able to provide new insights into the interannual variation in vegetation changing signals and play a key role in accurately modeling vegetation phenology or the seasonality of ecosystem processes.

4.3. Climatic Influences on Vegetation Asymmetries

Vegetation asymmetries are not traditional phenological parameters, but, nevertheless, they are characteristic of these parameters, and, in some regions, their interannual variability is undoubtedly influenced by climatic changes. Different asymmetric patterns may reflect adaptations of vegetation communities to specific climate conditions. In this study, a relative importance (RI) analysis suggests that precipitation plays a role equivalent to that of temperature on productivity. This finding differs

slightly from other reports that state that northern temperate ecosystems are primarily influenced by temperature and solar radiation [52–55]. In this case, the joint controlling effect of temperature and precipitation on variations in plant asymmetries may be attributed to their synchronous changes over time and space (see Figure 11). That joint control could be reflected in the similar spatial pattern of relative importance of AsyTemp and AsyPrpc to AsyV and AsyR (Figure 10). However, due to their low contributions, it is apparent that temperature and precipitation are not adequate constraints for asymmetry in growing season length (AsyL). For example, the inherent gene types of vegetation may limit the changing ranges of phenological events (e.g., SOS, EOS) and further affect changes in AsyL.

Based on the inter-comparison of averaged annual indices, a negative AsyTemp indicates a warmer spring. The growth rate asymmetry (AsyR) is generally positive (red and purple patches in Figure 12c), while AsyV tends to be negative (brown and light blue patches in Figure 12b). The reverse is true when AsyTemp is positive. This phenomenon reflects warming springs that can rapidly stimulate plant growth, resulting in a shorter growing season during green up and further reducing average greenness. When AsyPrpc is negative, AsyR tends to be positive and AsyV tends to be negative, which accounts for a large proportion of pixels. In this situation, sufficient water is available to improve the rate of plant activity (i.e., photosynthesis) across the NEC. As with the effect of AsyTemp on AsyV, this rapid plant growth leads to a smaller mean greenness during green up than during senescence. The effects of AsyTemp and AsyPrpc on AsyL show a relatively complex pattern, especially in the southern and eastern forest, where AsyTemp and AsyPrpc with positive values likely correspond to a positive AsyL, but with a considerable number of negative values (green grid cells).

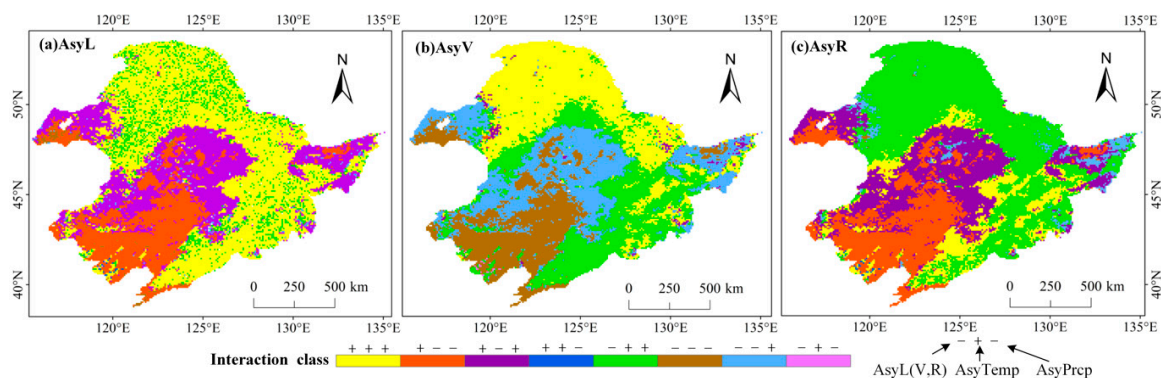


Figure 12. Spatial patterns of the influence of temperature and precipitation on vegetation asymmetries. This is an inter-comparison between average annual asymmetries of AsyL (AsyV, AsyR), AsyTemp and AsyPrpc. An interaction noted as ‘- + -’ successively represents negative AsyL (V, R), positive AsyTemp and negative AsyPrpc from the average annual mean.

The influence of warmer springs may affect subsequent seasons through the development of larger leaves or increased foliar nitrogen [53], which will result in enhanced carbon assimilation in the following summer and autumn. The temporal fluctuation of the magnitude and sign of vegetation asymmetries may affect the allocation of production during different seasons and even change ecological traits, such as mobility or reproduction, that are tightly linked to ecosystem stability and food security [22,56].

Shifts in vegetation growth asymmetry are driven predominantly by climate change and variability, yet these shifts will also have an impact on future climate change through feedbacks to the atmospheric system. It is noteworthy that crop growth cycles may be uniquely independent of a direct link the influence of natural forces. A variety of human-induced activities, such as planting time, irrigation and harvest time, can lead to different growth pattern for specific crops. Variability and changes in vegetation growth asymmetries for these crops could change land surface properties, such as LAI and albedo, resulting in local climatic changes [57]. The changing vegetation growth asymmetries may also affect carbon uptake process and further enhance seasonal CO₂ exchange in northern ecosystems [58]

4.4. Potential Limitation and the Way Forward

It should be noted that there will be diverse growth shapes for annual vegetation [21] that is not enumerated for all the possible types in this study. This paper simply focuses on the asymmetric status of plant seasonal growth for a temperate terrestrial ecosystem. The conceptual growth curves shown in Figure 2 aim to demonstrate a general growth process in NEC, but the asymmetric indices can quantitatively describe the vegetation development process from three dimensions. Additionally, there are a number of shape parameters that can depict time series curves [9,59,60]. Therefore, one asymmetric index may not necessarily correspond uniquely to a single specific seasonal growth curve. The combination of several key phenological events may be conducive to identifying a specific plant growth type. Moreover, although widely used, timing and growth rate asymmetries may be influenced by the curve fitting method and input data sources. High spatiotemporal resolution data, such as Sentinel2 and Phenocam camera data, will advance the accuracy of these vegetation asymmetries. Yet the applicability of asymmetric indices in other broader and various ecoregions remains unclear and required further validation.

For GIMMS NDVI3g dataset, the summer saturation effect of NDVI over dense forests (e.g., broad-leaved forests in eastern NEC and coniferous forests in Daxing'anling Mountains) may cause uncertainties in growth curve fitting and phenological parameters extraction. These uncertainties would primarily affect the absolute value of growing season length, green up rate, senescence rate and average NDVI in spring and autumn. But the asymmetric indices are defined as the difference between these variables that may offset some uncertainties. In the future work, the non-saturated vegetation index (e.g., EVI) will be employed to optimize these asymmetric indices. Regarding the climatic impacts on vegetation asymmetries, the time-lag effect of temperature and rainfall on vegetation growth is very critical but not estimated in this study. The future work will consider this effect.

5. Summary and Conclusions

This study focused on the diversity between green up and senescent segments of vegetation greenness seasonal cycles, which correspond to periods when terrestrial ecosystems generally release and uptake carbon dioxide, respectively. Therefore, a set of vegetation asymmetries in growth length (AsyL), vegetation greenness (AsyV) and growth rate (AsyR) were defined to characterize detailed differences in vegetation growth shapes during the two halves of the growing season. Long-term trends and the spatial distribution of these asymmetric indices were analyzed. Conclusion are drawn as follows.

- (1) For the long term, the asymmetric indices of vegetation growth in Northeast China have significant interannual variability with an approximate periodicity of ten years, especially for AsyR and AsyV. The total time series of AsyV and AsyL exhibit a synchronous profile that is opposite to that of AsyR. Spatially, the average annual values and long-term trends of AsyR and AsyV are arranged with clear cluster patches that are approximately consistent with the geographic distribution of primary vegetation cover types. The AsyL, nevertheless, shows a relatively complex spatiotemporal pattern. AsyR reveals that the senescence rate in cropland and grassland was faster than the green up rate, while the opposite was true for the forest types. Trends in AsyL indicate that all plant types show a longer growing season in the senescent phase than the green up phase. However, spring mean greenness is much greater than autumn greenness in all vegetation types, except conifer forest.

- (2) The combined effects of climatic constraints on vegetation asymmetries are pronounced when viewed both spatially and temporally. Asymmetries in temperature (AsyTemp) and rainfall (AsyPrcp) show similar temporal profiles as the vegetation asymmetries, and they jointly control changes in the three asymmetrical indices, with a roughly equivalent contribution identified by the relative importance (RI) analysis. AsyTemp and AsyPrcp contribute more to changes in AsyR and AsyV than in AsyL, while climatic asymmetries are negatively linked to AsyR, but positively correlated to AsyV and AsyL. Overall, these asymmetric indices provide for the potential to effectively depict detailed seasonal states of vegetation growth. Shifts of magnitude and sign in vegetation asymmetries over Northeast China follow a certain pattern in location and time, which helps us to understand the seasonal cycle of these terrestrial ecosystems. In future research, it will be necessary to derive more shape parameters of plant growth cycles to combine with other observed vegetation bio-physiological (such as GPP, LAI, FPAR and flux) and model data to reveal the influence of asymmetry on vegetation seasonal processes.

Funding: This research was funded by National Natural Science Foundation of China grant number 41601478 and National Key Research and Development Program grant numbers 2018YFB0505301, 2016YFC0500103. The APC was funded by 2018YFB0505301, 2016YFC0500103.

Conflicts of Interest: The author declares no conflict of interest.

References

1. Wang, X.; Xiao, J.; Li, X.; Cheng, G.; Ma, M.; Zhu, G.; Arain, M.A.; Black, T.A.; Jassal, R.S. No trends in spring and autumn phenology during the global warming hiatus. *Nat. Commun.* **2019**, *10*, 2389. [[CrossRef](#)] [[PubMed](#)]
2. Menzel, A.; Sparks, T.H.; Estrella, N.; Koch, E.; Aasa, A.; Ahas, R.; Alm-Kübler, K.; Bissolli, P.; Braslavská, O.; Briede, A. European phenological response to climate change matches the warming pattern. *Glob. Chang. Biol.* **2006**, *12*, 1969–1976. [[CrossRef](#)]
3. Körner, C.; Basler, D. Phenology under global warming. *Science* **2010**, *327*, 1461–1462. [[CrossRef](#)] [[PubMed](#)]
4. Schwartz, M.D.; Ahas, R.; Aasa, A. Onset of spring starting earlier across the Northern Hemisphere. *Glob. Chang. Biol.* **2006**, *12*, 343–351. [[CrossRef](#)]
5. Jeong, S.; HO, C.; GIM, H.; Brown, M.E. Phenology shifts at start vs. end of growing season in temperate vegetation over the Northern Hemisphere for the period 1982–2008. *Glob. Chang. Biol.* **2011**, *17*, 2385–2399. [[CrossRef](#)]
6. Vrieling, A.; Meroni, M.; Darvishzadeh, R.; Skidmore, A.K.; Wang, T.; Zurita-Milla, R.; Oosterbeek, K.; O'Connor, B.; Paganini, M. Vegetation phenology from Sentinel-2 and field cameras for a Dutch barrier island. *Remote Sens. Environ.* **2018**, *215*, 517–529. [[CrossRef](#)]
7. Zeng, H.; Jia, G.; Epstein, H. Recent changes in phenology over the northern high latitudes detected from multi-satellite data. *Environ. Res. Lett.* **2011**, *6*, 45508. [[CrossRef](#)]
8. Julien, Y.; Sobrino, J.A. Global land surface phenology trends from GIMMS database. *Int. J. Remote Sens.* **2009**, *30*, 3495–3513. [[CrossRef](#)]
9. Zhang, X.; Friedl, M.A.; Schaaf, C.B.; Strahler, A.H.; Hodges, J.C.F.; Gao, F.; Reed, B.C.; Huete, A. Monitoring vegetation phenology using MODIS. *Remote Sens. Environ.* **2003**, *84*, 471–475. [[CrossRef](#)]
10. White, M.A.; Thornton, P.E.; Running, S.W. A continental phenology model for monitoring vegetation responses to interannual climatic variability. *Glob. Biogeochem. Cycles* **1997**, *11*, 217–234. [[CrossRef](#)]
11. Richardson, A.D.; Keenan, T.F.; Migliavacca, M.; Ryu, Y.; Sonnentag, O.; Toomey, M. Climate change, phenology, and phenological control of vegetation feedbacks to the climate system. *Agric. For. Meteorol.* **2013**, *169*, 156–173. [[CrossRef](#)]
12. Fu, Y.H.; Zhao, H.; Piao, S.; Peaucelle, M.; Peng, S.; Zhou, G.; Ciais, P.; Huang, M.; Menzel, A.; Peñuelas, J. Declining global warming effects on the phenology of spring leaf unfolding. *Nature* **2015**, *526*, 104. [[CrossRef](#)] [[PubMed](#)]
13. Keenan, T.F.; Gray, J.; Friedl, M.A.; Toomey, M.; Bohrer, G.; Hollinger, D.Y.; Munger, J.W.; O'Keefe, J.; Schmid, H.P.; Wing, I.S. Net carbon uptake has increased through warming-induced changes in temperate forest phenology. *Nat. Clim. Chang.* **2014**, *4*, 598. [[CrossRef](#)]

14. Richardson, A.D.; Hufkens, K.; Milliman, T.; Aubrecht, D.M.; Chen, M.; Gray, J.M.; Johnston, M.R.; Keenan, T.F.; Klosterman, S.T.; Kosmala, M. Tracking vegetation phenology across diverse North American biomes using PhenoCam imagery. *Sci. Data* **2018**, *5*, 180028. [[CrossRef](#)] [[PubMed](#)]
15. Zhu, Z.; Piao, S.; Myneni, R.B.; Huang, M.; Zeng, Z.; Canadell, J.G.; Ciais, P.; Sitch, S.; Friedlingstein, P.; Arneeth, A. Greening of the Earth and its drivers. *Nat. Clim. Chang.* **2016**, *6*, 791. [[CrossRef](#)]
16. Richardson, A.D.; Hufkens, K.; Milliman, T.; Aubrecht, D.M.; Furze, M.E.; Seyednasrollah, B.; Krassovski, M.B.; Latimer, J.M.; Nettles, W.R.; Heiderman, R.R. Ecosystem warming extends vegetation activity but heightens vulnerability to cold temperatures. *Nature* **2018**, *560*, 368. [[CrossRef](#)]
17. Huang, K.; Xia, J.; Wang, Y.; Ahlström, A.; Chen, J.; Cook, R.B.; Cui, E.; Fang, Y.; Fisher, J.B.; Huntzinger, D.N. Enhanced peak growth of global vegetation and its key mechanisms. *Nat. Ecol. Evol.* **2018**, *2*, 1897. [[CrossRef](#)]
18. Calle, L.; Poulter, B.; Patra, P.K. A segmentation algorithm for characterizing rise and fall segments in seasonal cycles: An application to XCO₂ to estimate benchmarks and assess model bias. *Atmos. Meas. Tech.* **2019**, *12*, 2611–2629. [[CrossRef](#)]
19. Cohen, J.L.; Furtado, J.C.; Barlow, M.; Alexeev, V.A.; Cherry, J.E. Asymmetric seasonal temperature trends. *Geophys. Res. Lett.* **2012**, *39*. [[CrossRef](#)]
20. Beck, P.S.A.; Atzberger, C.; Høgda, K.A.; Johansen, B.; Skidmore, A.K. Improved monitoring of vegetation dynamics at very high latitudes: A new method using MODIS NDVI. *Remote Sens. Environ.* **2006**, *100*, 321–334. [[CrossRef](#)]
21. Gu, L.; Post, W.M.; Baldocchi, D.D.; Black, T.A.; Suyker, A.E.; Verma, S.B.; Vesala, T.; Wofsy, S.C. Characterizing the seasonal dynamics of plant community photosynthesis across a range of vegetation types. In *Phenology of Ecosystem Processes*; Springer: Berlin/Heidelberg, Germany, 2009; pp. 35–58.
22. Fitchett, J.M.; Grab, S.W.; Thompson, D.I. Plant phenology and climate change: Progress in methodological approaches and application. *Prog. Phys. Geogr.* **2015**, *39*, 460–482. [[CrossRef](#)]
23. Piao, S.; Fang, J.; Zhou, L.; Ciais, P.; Zhu, B. Variations in satellite-derived phenology in China's temperate vegetation. *Glob. Chang. Biol.* **2006**, *12*, 672–685. [[CrossRef](#)]
24. Chen, X.; Hu, B.; Yu, R. Spatial and temporal variation of phenological growing season and climate change impacts in temperate eastern China. *Glob. Chang. Biol.* **2005**, *11*, 1118–1130. [[CrossRef](#)]
25. Cong, N.; Piao, S.; Chen, A.; Wang, X.; Lin, X.; Chen, S.; Han, S.; Zhou, G.; Zhang, X. Spring vegetation green-up date in China inferred from SPOT NDVI data: A multiple model analysis. *Agric. For. Meteorol.* **2012**, *165*, 104–113. [[CrossRef](#)]
26. Xiao, X.; Boles, S.; Liu, J.; Zhuang, D.; Liu, M. Characterization of forest types in Northeastern China, using multi-temporal SPOT-4 VEGETATION sensor data. *Remote Sens. Environ.* **2002**, *82*, 335–348. [[CrossRef](#)]
27. Wang, J.X.L.; Gaffen, D.J. Late-twentieth-century climatology and trends of surface humidity and temperature in China. *J. Clim.* **2001**, *14*, 2833–2845. [[CrossRef](#)]
28. Yu, X.; Zhuang, D.; Hou, X.; Chen, H. Forest phenological patterns of Northeast China inferred from MODIS data. *J. Geogr. Sci.* **2005**, *15*, 239–246. [[CrossRef](#)]
29. Tucker, C.J.; Pinzon, J.E.; Brown, M.E.; Slayback, D.A.; Pak, E.W.; Mahoney, R.; Vermote, E.F.; El Saleous, N. An extended AVHRR 8-km NDVI dataset compatible with MODIS and SPOT vegetation NDVI data. *Int. J. Remote Sens.* **2005**, *26*, 4485–4498. [[CrossRef](#)]
30. Pinzon, J.; Tucker, C. A non-stationary 1981–2012 AVHRR NDVI3g time series. *Remote Sens.* **2014**, *6*, 6929–6960. [[CrossRef](#)]
31. Tian, F.; Fensholt, R.; Verbesselt, J.; Grogan, K.; Horion, S.; Wang, Y. Evaluating temporal consistency of long-term global NDVI datasets for trend analysis. *Remote Sens. Environ.* **2015**, *163*, 326–340. [[CrossRef](#)]
32. Myneni, R.B.; Keeling, C.D.; Tucker, C.J.; Asrar, G.; Nemani, R.R. Increased plant growth in the northern high latitudes from 1981 to 1991. *Nature* **1997**, *386*, 698. [[CrossRef](#)]
33. Wang, J.; Ye, H.; Liu, Y.; He, H. An interpolated temperature and precipitation dataset at 1-km grid resolution in China (2000–2012). *China Sci. Data* **2017**, *2*, 88–95.
34. Forkel, M.; Wutzler, T. Greenbrown—Land Surface Phenology and Trend Analysis. *A Packag. R Softw. Version* **2015**, *2*, 15.
35. Sayemuzzaman, M.; Jha, M.K. Seasonal and annual precipitation time series trend analysis in North Carolina, United States. *Atmos. Res.* **2014**, *137*, 183–194. [[CrossRef](#)]
36. Mann, H.B. Nonparametric tests against trend. *Econom. J. Econom. Soc.* **1945**, 245–259. [[CrossRef](#)]
37. Kendall, M.G. *Rank Correlation Methods*; Hafner: New York, NY, USA, 1962.

38. Myers, L.; Sirois, M.J. Spearman correlation coefficients, differences between. *Encycl. Stat. Sci.* **2004**, *12*. [[CrossRef](#)]
39. Zar, J.H. Significance testing of the Spearman rank correlation coefficient. *J. Am. Stat. Assoc.* **1972**, *67*, 578–580. [[CrossRef](#)]
40. Grömping, U. Relative importance for linear regression in R: The package relaimpo. *J. Stat. Softw.* **2006**, *17*, 1–27. [[CrossRef](#)]
41. Lindeman, R.H. *Introduction to Bivariate and Multivariate Analysis*; Scott, Foresman & Co.: Glenview, IL, USA, 1980.
42. Hyndman, R.J.; Khandakar, Y. *Automatic Time Series for Forecasting: The Forecast Package for R*; Monash University, Department of Econometrics and Business Statistics: Melbourne, VIC, Australia, 2007.
43. Medhaug, I.; Stolpe, M.B.; Fischer, E.M.; Knutti, R. Reconciling controversies about the ‘global warming hiatus’. *Nature* **2017**, *545*, 41. [[CrossRef](#)] [[PubMed](#)]
44. Fyfe, J.C.; Meehl, G.A.; England, M.H.; Mann, M.E.; Santer, B.D.; Flato, G.M.; Hawkins, E.; Gillett, N.P.; Xie, S.-P.; Kosaka, Y. Making sense of the early-2000s warming slowdown. *Nat. Clim. Chang.* **2016**, *6*, 224. [[CrossRef](#)]
45. Randerson, J.T.; Thompson, M.V.; Conway, T.J.; Fung, I.Y.; Field, C.B. The contribution of terrestrial sources and sinks to trends in the seasonal cycle of atmospheric carbon dioxide. *Glob. Biogeochem. Cycles* **1997**, *11*, 535–560. [[CrossRef](#)]
46. Barnett, T.P.; Adam, J.C.; Lettenmaier, D.P. Potential impacts of a warming climate on water availability in snow-dominated regions. *Nature* **2005**, *438*, 303. [[CrossRef](#)] [[PubMed](#)]
47. Simonetti, E.; Simonetti, D.; Preatoni, D. Phenology-based land cover classification using Landsat 8 time series. *Eur. Comm. Jt. Res. Cent. Ispra Italy* **2014**. [[CrossRef](#)]
48. Götze, C.; Gerstmann, H.; Gläßer, C.; Jung, A. An approach for the classification of pioneer vegetation based on species-specific phenological patterns using laboratory spectrometric measurements. *Phys. Geogr.* **2017**, *38*, 524–540. [[CrossRef](#)]
49. Kiptala, J.K.; Mohamed, Y.; Mul, M.L.; Cheema, M.J.M.; Van der Zaag, P. Land use and land cover classification using phenological variability from MODIS vegetation in the Upper Pangani River Basin, Eastern Africa. *Phys. Chem. Earth Parts ABC* **2013**, *66*, 112–122. [[CrossRef](#)]
50. Li, F.; Liu, Z.; Han, L.; Yinyou, H.; Peijun, D.; Adaku, E. Urban vegetation classification based on phenology using HJ-1A/B time series imagery. In Proceedings of the 2015 Joint Urban Remote Sensing Event (JURSE), Lausanne, Switzerland, 30 March–1 April 2015; pp. 1–4.
51. Yan, E.; Wang, G.; Lin, H.; Xia, C.; Sun, H. Phenology-based classification of vegetation cover types in Northeast China using MODIS NDVI and EVI time series. *Int. J. Remote Sens.* **2015**, *36*, 489–512. [[CrossRef](#)]
52. Kim, Y.; Kimball, J.S.; Didan, K.; Henebry, G.M. Response of vegetation growth and productivity to spring climate indicators in the conterminous United States derived from satellite remote sensing data fusion. *Agric. For. Meteorol.* **2014**, *194*, 132–143. [[CrossRef](#)]
53. Buermann, W.; Forkel, M.; O’Sullivan, M.; Sitch, S.; Friedlingstein, P.; Haverd, V.; Jain, A.K.; Kato, E.; Kautz, M.; Lienert, S. Widespread seasonal compensation effects of spring warming on northern plant productivity. *Nature* **2018**, *562*, 110. [[CrossRef](#)]
54. Garonna, I.; de Jong, R.; Stöckli, R.; Schmid, B.; Schenkel, D.; Schimel, D.; Schaepman, M.E. Shifting relative importance of climatic constraints on land surface phenology. *Environ. Res. Lett.* **2018**, *13*, 24025. [[CrossRef](#)]
55. Nemani, R.R.; Keeling, C.D.; Hashimoto, H.; Jolly, W.M.; Piper, S.C.; Tucker, C.J.; Myneni, R.B.; Running, S.W. Climate-driven increases in global terrestrial net primary production from 1982 to 1999. *Science* **2003**, *300*, 1560–1563. [[CrossRef](#)]
56. Brown, C.J.; O’Connor, M.I.; Poloczanska, E.S.; Schoeman, D.S.; Buckley, L.B.; Burrows, M.T.; Duarte, C.M.; Halpern, B.S.; Pandolfi, J.M.; Parmesan, C. Ecological and methodological drivers of species’ distribution and phenology responses to climate change. *Glob. Chang. Biol.* **2016**, *22*, 1548–1560. [[CrossRef](#)] [[PubMed](#)]
57. Peñuelas, J.; Filella, I. Phenology feedbacks on climate change. *Science* **2009**, *324*, 887–888. [[CrossRef](#)] [[PubMed](#)]
58. Forkel, M.; Carvalhais, N.; Rödenbeck, C.; Keeling, R.; Heimann, M.; Thonicke, K.; Zaehle, S.; Reichstein, M. Enhanced seasonal CO₂ exchange caused by amplified plant productivity in northern ecosystems. *Science* **2016**, *351*, 696–699. [[CrossRef](#)] [[PubMed](#)]

59. Klosterman, S.; Hufkens, K.; Gray, J.M.; Melaas, E.; Sonnentag, O.; Lavine, I.; Mitchell, L.; Norman, R.; Friedl, M.A.; Richardson, A. Evaluating remote sensing of deciduous forest phenology at multiple spatial scales using PhenoCam imagery. *Biogeosciences* **2014**. [[CrossRef](#)]
60. Kramer, K.; Hänninen, H. The annual cycle of development of trees and process-based modelling of growth to scale up from the tree to the stand. In *Phenology of Ecosystem Processes*; Springer: Berlin/Heidelberg, Germany, 2009; pp. 201–227.



© 2019 by the author. Licensee MDPI, Basel, Switzerland. This article is an open access article distributed under the terms and conditions of the Creative Commons Attribution (CC BY) license (<http://creativecommons.org/licenses/by/4.0/>).